Articles

Novel Chain and Oligomeric Condensed Cluster Phases for Gadolinium Iodides with Manganese Interstitials

Masahiro Ebihara, James D. Martin, and John D. Corbett*

Department of Chemistry, Iowa State University, Ames, Iowa 50011

Received July 28, 1993®

Reactions in the Gd–I–Mn system near 800 °C in sealed Nb containers provide good yields of Gd_3I_3Mn and Gd_5I_7Mn. The first is isostructural with the Pr_3I_3Ru family ($P2_1/m$, $Z = 2$, $a = 8.928(3)$ Å, $b = 4.127(1)$ Å, $c = 12.266(4)$ Å, $\beta = 95.51(2)°$; R, $R_w = 4.1$, 4.8%). The Gd_5I_7Mn phase has a new cubic structure ($P\bar{4}3m$, $Z = 4$, $a = 12.1765(1)$ Å; R, $R_w = 3.5$, 3.4%). Both structures exhibit substantially shorter Mn–Mn interactions than seen before with electron-richer interstitials. Distorted double chains of edge-sharing Gd_6Mn octahedra in Gd_3I_3Mn resemble those in $Y_3I_3(Ru,Ir)$, but with 2.66-Å separations in a distinct zigzag Mn chain within. The new Gd_5I_7Mn contains two types of clusters: (a) $Gd_{16}I_{20}Mn_4$ units that closely resemble the Ru_4-centered tetracapped truncated tetrahedron Y_{16} in $Y_{16}I_{20}Ru_4$ but with strong Mn displacements to $\bar{d}$(Mn–Mn) = 2.825 Å in the centered tetrahedra; (b) Gd_4I_8 capped tetrahedra interbonded with those of type a which have ~25% of each metal vertex displaced outward in a disordered manner. The small type b clusters appear to be oxidized to give a $(Gd_4I_8)^{4+}[Gd_{16}(Mn)_4I_{20}]^{4-}$ formulation. Calculations suggest this arrangement does not give a closed configuration with these elements, perhaps because of the stoichiometry limitations with a single type of interstitial.

Introduction

A fascinating variety of cluster and condensed cluster halides of the rare-earth metals (R) have been discovered in which every cluster is centered by a heteroelement (Z) as an interstitial. Those with a heterometal Z are some of the most novel since they afford so many intermetal bonding examples. For instance, isolated $R_6I_{12}Z$-type clusters are known in $R_7I_{12}Z$ or $R_6I_{10}Z$ compositions for Z = Mn–Cu, Ru–Pd, and Re–Au with R = Y, Pr, Gd (and presumably others).[1-4] These same systems also afford numerous condensed cluster phases in the form of infinite chains, double chains, or interlinked networks with R_4I_5Z,[5,6] R_4Br_4Os,[7] and R_3I_3Z[8,9] compositions. However, the range of interstitial atoms possible in each seems to be much more limited than in isolated clusters. Collectively, only Fe, Co, Ni, Ru, Os, Ir, and Pt have previously been observed in condensed cluster phases.

One particular series, the monoclinic R_3I_3Z, contains infinite double chains of R_6Z octahedra, that is, single trans-edge-sharing chains that are further cocondensed in pairs. These have previously been found only for Z = Ru and Ir with R ranges from at least Pr to Er and Y, suggesting much more restricted electronic conditions for stability. In addition, a smaller R, or the marginally larger and electron-richer interstitial Ir, causes a continuous distortion of the structure by which cluster pairs within the double chain merge and virtually disappear as building blocks. This same process causes a notable decrease in the Z–Z separations, although these still remain weakly bonded at best (Pauling bond order ≤0.10) in the prior examples.[9] Surprisingly, only one example of an oligomeric phase has been reported. The tetrameric $(Y_4I_5Ru)_4$ contains four Y_6Ru clusters condensed so as to share edges in a tetrahedral manner, such that the yttrium arrangement can be described as a tetracapped truncated tetrahedron or icosioctahedron. The Ru–Ru bonding appears to be very weak.[10]

We have now discovered gadolinium–manganese analogues of both the monoclinic chain phase R_3I_3Z and the oligomeric $Y_{16}I_{20}Ru_4$, the latter somewhat elaborated. A description of the structure of and bonding within these, in which the smaller and electron-poorer interstitial Mn affords significant distortion and clearly greater Z–Z interactions, follows.

Experimental Section

Syntheses. Exploration of Gd–I–Z systems was prompted by a desire to find better crystals of one or more incompletely characterized phases that occur near a Gd_4I_4Z composition. Reactions with overall stoichiometries Gd_4I_4Mn that were run as before[1-3] in sealed Nb containers and explored the range of 750–900 °C for 2–4 weeks produced products with relatively complex powder patterns. Major amounts of one new phase (60–70%) could be identified by powder pattern as well as the previously known $Gd_7I_{12}Mn$[3] and small amounts of an acicular Gd_3I_3Mn that was seemingly isostructural with monoclinic Y_3I_3Ru.[9] Unreacted Gd was always present, and the first new phase disappeared from the products after reactions at 900 °C or above. This black cube-shaped material from a reaction at 850 °C for 4 weeks was shown to be Gd_5I_7Mn. Stoichiometric reaction compositions at 800 °C produced Gd_5I_7Mn in fair yield together with 70% $Gd_7I_{12}Mn$, perhaps because of adventitious oxidation accompanied by the formation of small amounts of the inevitable GdOI. One or more unidentified products also appeared at 850 °C. A sensitivity of product distributions to temperature, and perhaps time, in some of these complex systems has been noted before.[5,11] Other Z prospects, including Re, gave only previously known phases.

Both structures were determined from room temperature diffraction data collected to 2θ limits of 50 and 65° on a Rigaku AFC-6R

* Abstract published in *Advance ACS Abstracts*, April 1, 1994.

(1) Hughbanks, T.; Corbett, J. D. *Inorg. Chem.* **1988**, *27*, 2022.
(2) Hughbanks, T.; Corbett, J. D. *Inorg. Chem.* **1989**, *28*, 631.
(3) Payne, M. W.; Corbett, J. D. *Inorg. Chem.* **1990**, *29*, 2246.
(4) Simon, A.; Mattausch, Hj.; Miller, G. J.; Bauhofer, W.; Kremer, R. K. In *Handbook on the Physics and Chemistry of Rare Earths*, Gschneidner, K. A., Eyring, L., Eds., North-Holland; Amsterdam, 1991; Vol. 15, pp 191–285.
(5) Payne, M. W.; Dorhout, P. K.; Corbett, J. D. *Inorg. Chem.* **1990**, *30*, 1467, 3112.
(6) Park, Y.; Corbett, J. D. Unpublished research.
(7) Dorhout, P. K.; Corbett, J. D. *J. Am. Chem. Soc.* **1992**, *14*, 497.
(8) Dorhout, P. K.; Payne, M. W.; Corbett, J. D. *Inorg. Chem.* **1991**, *30*, 4960.
(9) Payne, M. W.; Dorhout, P. K.; Kim, S.-J.; Hughbanks, T. R.; Corbett, J. D. *Inorg. Chem.* **1992**, *32*, 1389.
(10) Payne, M. W.; Ebihara, M.; Corbett, J. D. *Angew. Chem., Int. Ed. Engl.*, **1991**, *30*, 856.
(11) Llusar, R.; Corbett, J. D. *Inorg. Chem.* **1994**, *33*, 849.

0020-1669/94/1333-2079$04.50/0

Table 1. Selected Single Crystal Data Collection and Refinement Parameters

formula	Gd_3I_3Mn	Gd_5I_7Mn
space group, Z	$P2_1/m$ (No. 11), 2	$P\bar{4}3m$ (No. 215), 4
lattice params[a]		
a, Å	8.928 (3)	12.1765 (1)
b, Å	4.127 (1)	
c, Å	12.266 (4)	
β, deg	95.51 (2)	
no. unique reflcns;[b] $2\theta_{max}$ deg	745; 50	1018; 65
μ(Mo Kα), cm^{-1}	333.8	306.8
trans factor range (scaled)	0.782–1.164	0.721–1.128
no. of params	44	35
R,[c] %	4.1	3.5
R_w,[d] %	4.8	3.4

[a] Guinier powder data with Si as internal standard; λ = 1.540 562 Å. [b] $F_o/\sigma_F > 3.0$. [c] $R = \sum||F_o|-|F_c||/\sum|F_o|$. [d] $R_w = [\sum w(|F_o|-|F_c|)^2/\sum w(F_o)^2]^{1/2}$; $w = \sigma_F^{-2}$.

diffractometer using Mo Kα radiation. The accompanying program package (TEXSAN) was used for data processing and structure refinements. A summary of the conditions of data collection and structure refinement is given in Table 1. Structure factor data are available from J.D.C.

Gd_3I_3Mn. One reflection in the initial orientation set indicated a c axis length of 24.46 Å, twice that expected on the basis of the supposed structural analogues (Y_3I_3Ru, etc.), and so a hemisphere of data was collected. Nevertheless, only 62 reflections with odd l remained out of 807 after equivalent reflections were averaged in the consistent and forecasted space group $P2_1/m$. Direct methods (SHELX) gave all atomic positions in a model in which two independent chains along $\vec{b}$ lay about different $\bar{1}$ sites (0, 0, $^1/_2$ and 0, $^1/_2$, $^1/_2$, etc.). However, refinements of this model gave serious coupling troubles between both positions and temperature factors of most atoms that would be symmetry equivalent in the normal cell, and the R value for the generally weak reflections with l odd was 39% (isotropic) while that for all observed data was 5.8%. These so-called peaks were generally next to strong peaks with l even, and a subsequent zero-level Weissenberg photograph shows no evidence of the larger cell. Assumption of the normal cell yielded R_{av} = 6.0% for all data, and this dropped to 3.1% after absorption corrections by DIFABS which is based on symmetry equivalent reflections.[12] The latter correction also decreased the U_{22} values for all atoms by 35–40%, a reasonable and not uncommon result when absorption by the needle crystal growing along $\vec{b}$ had been previously corrected only by ψ-scans. All parameters were reasonable and well-behaved at convergence (R = 4.1%). The largest residual in the difference Fourier map was a 2.0 e/Å^3 peak that was 2.2 Å from Gd2.

Gd_5I_7Mn. Although the powder pattern of this phase looked something like that of the bcc Ca_3PI_3 type [as known for $(La,Pr)_3I_3(Os,Ir,Pt)$[8]], extra lines were present. Oscillation and Weissenberg photographs of one of the cube-shaped crystals indicated a primitive cubic cell and probable space groups $P\bar{4}3m$, $P432$, or $Pm\bar{3}m$. The diffractometer programs predicted the corresponding $m\bar{3}m$ Laue symmetry, while processing of two octants of diffraction data indicated the asymmetric choice $P\bar{4}3m$. The data were so averaged (exempting Friedel pairs) after a ψ-scan correction for absorption. Direct methods at this point did not give a suitable solution, but investigations with other space groups in Laue class $m\bar{3}$ resulted in a direct-methods solution in $Pm\bar{3}$. However, the refined positions obtained therefrom indicated that $P\bar{4}3m$ was apparently correct, and the resulting seven atoms refined well to R = 5.1% (isotropic). At this point, the isolated Gd3 atom showed a much larger (and disparate) ellipsoid, and a ΔF map indicated a large adjoining peak of ~13 e/Å^3. Splitting this position into Gd31 (major) and Gd32 gave a good solution with the first data set. Refinement of occupancies of the two Gd3 members without restriction (and fixed B_{iso}) gave a sum close to unity and proportions close to 3:1, so the first condition was imposed thereafter. A second data set collected for another crystal on a CAD4 diffractometer (to $2\theta \leq 50°$) gave the same result (R/R_w = 3.8/4.5%, with somewhat larger errors) so the effect was assumed to be real. DIFABS correction for adsorption[12] reduced the parameter errors 20–28%. The introduction of Gd32 amounts to a 0.77(1)-Å displacement of ca. 25% of each vertex of a large Gd3 tetrahedron outward along the 3-fold axes, and this creates otherwise short Gd32-I2 distances (see Results). However, the difference Fourier map clearly showed a secondary I22 peak 0.26 Å from I21 that had appropriate distances to the metals and frequency. Introduction of this minor image (at 1:3) refined well, and gave plausible distances all around (R_{iso} ≃ 3.8%). The multiple disorder expected for I3 as well (evident in ΔF and its B) could not be resolved at a sensible level, consistent with the final analysis. The largest residual ΔF peak at convergence, 3.5 e/Å^3, was 0.41 Å from Gd2. The correct configuration was identified by comparison of F_o with F_c for ~60 instances in which the enantiomeric choice had the larger effects on F_c. A total of 62 indexed reflections from the Guinier powder pattern yielded a cubic lattice constant of 12.1765(1) Å.

The nature of the structure refined (see Results: Gd_5I_7Mn) suggested that the unusual disorder, a 1-in-4 displacement of all four metal vertices in a Gd_4I_8 tetrahedron, could be introduced into a unique model either by twinning or by incorrect refinement of a rhombohedral structure in the cubic group. Therefore, the original reflection data set and the first seven atoms located for the cubic cell were also transformed into the other three possible orientations of a unique 3-fold axes for the consistent $R3m$ space group (No. 160), and each of the four data sets averaged and refined in the rhombohedral setting.

More-or-less the same 17-atom model resulted in all cases at R_{iso} ~ 7%. The displaced Gd32 equivalents were always evident in Fourier maps as well as, subsequently, most of the corresponding second I2 members. These groups of atoms were successively introduced into the two data sets where the greater extremes in proportions were apparent, and these refined isotropically with intervening maps as before to R_{iso} ~ 6% with no unreasonable distances. Although only disordered models were still obtained, a significant difference appeared in the proportions of normal and outwardly displaced Gd3-like components. These each occur as a 3b (m) and 1a ($3m$) pair in $R3m$ rather than the single 4e ($3m$) collection in $P\bar{4}3m$. The refined proportions of these two varied from 33% in 1a for the displaced atom (and less in the major) for one rhombohedral data set to 20% in 1a for the major Gd3 position in another. These differences suggest there are observably different proportions of what could be viewed as four orientations of a uniaxial rhombohedral structure in a quadrilled cubic crystal (pseudomerohedral twinning).

Extended Hückel Calculations. Extended Hückel calculations were performed on the $Gd_{16}I_{20}Mn_4^{4-}$ cluster with coordinates taken from the crystal structure as well as on a model cluster in which the Mn atom positions were shifted (Mn–Mn = 3.44 Å) to more closely represent the structure observed previously for $Y_{16}I_{20}Ru_4$. Calculations on the Gd_{16} and Mn_4 fragments were performed, as well as a band calculation at selected k points for the entire structure. The input energy parameters for Gd and Mn[13] were derived from self-consistent charge-iterative calculations on the hypothetical $Gd_6I_{18}Mn^{11-}$ model cluster with average distances from the crystal structure and the appropriate capping exo iodine at each vertex.

Results and Discussion

The positional parameters and isotropic-equivalent thermal parameters for Gd_3I_3Mn and Gd_5I_7Mn are given in Table 2. The two structures will be considered separately.

Gd_3I_3Mn. This structure type can be viewed as originating from chains of trans-edge-sharing Gd_6Mn octahedra that are further condensed through a pair-wise sharing of side edges. These units are sheathed by iodine atoms that bridge all exposed cluster edges and interbridge between chains. This phase is thus the eighth member of the monoclinic structure type R_3I_3Z; the other phases include R = La, Pr, Gd, Er, Y but only for Z = Ru or Ir.[9] Within this structure type there is considerable structural variation such that at one extreme the double chains interpenetrate enough that the original octahedra become difficult to recognize. Previously it was observed that the distortions increase with a decrease in the size of R, and, within the limited sample, with a larger Z (Ir), and that they parallel the axial a/b ratio fairly well. No obvious distortion attributable to the difference of one in the electron count between Ru and Ir was observed. The present

(12) Walker, N.; Stuart, D. *Acta Crystallogr.* **1983**, *A39*, 158.

(13) Input parameters for extended Hückel calculations (H_{ii}'s, Slater exponents (coefficients)): Gd 6s, –6.15 eV, 1.37; 6p, –3.05 eV, 1.37; 5d, –7.34 eV, 2.75 (0.7144) 1.26 (0.4560). Mn 4s, –7.24 eV, 1.80; 4p, –4.71 eV, 1.80; 3d, –7.57 eV, 5.15 (0.5139) 1.70 (0.6929). I 5s, –18.0 eV, 2.68; 5p, –12.17 eV, 2.32. Orbital parameters were taken from the "Tables of Parameters for Extended Hückel Calculations" collected by Santiago Alvarez, University of Barcelona, Spain, 1989.

Table 2. Positional Parameters and B_{eq} for Gd_3I_3Mn and Gd_5I_7Mn

atom	x	y	z	B_{eq},[a] Å^2
		Gd_3I_3Mn		
Gd1	0.1647(2)	1/4	0.8578(1)	0.85(7)
Gd2	0.0930(2)	1/4	0.3209(1)	0.94(7)
Gd3	0.2645(2)	3/4	0.1077(1)	1.00(7)
I1	0.4415(2)	3/4	0.8620(2)	1.4(1)
I2	0.3541(2)	3/4	0.3684(2)	1.22(9)
I3	0.1492(2)	1/4	0.6001(2)	1.21(9)
Mn	0.0299(5)	1/4	0.0673(4)	1.0(2)
		Gd_5I_7Mn		
Gd1 (12i)	0.11504(5)	x	0.32288(6)	0.62(1)
Gd2 (4e)	−0.14235(7)	x	x	0.4978(3)
Gd31[b] (4e)	0.3883(1)	x	x	1.5918(4)
Gd32[b] (4e)	0.3521(5)	x	x	2.448(2)
I1 (12i)	0.13300(8)	x	0.59775(9)	0.92(2)
I21 (12i)	0.3705(3)	x	0.1268(3)	1.13(6)
I22 (12i)	0.3724(8)	x	0.1057(8)	0.7(1)
I3 (4e)	−0.3660(1)	x	x	2.332(6)
Mn (4e)	0.0821(2)	x	x	0.4120(8)

[a] $B_{eq} = (8\pi^2/3)\sum_i\sum_j U_{ij}a_i^*a_j^*\vec{a}_i\vec{a}_j$. [b] Occupancies: Gd31 = 75.9(6)%, Gd32 = 24.1(6)%.

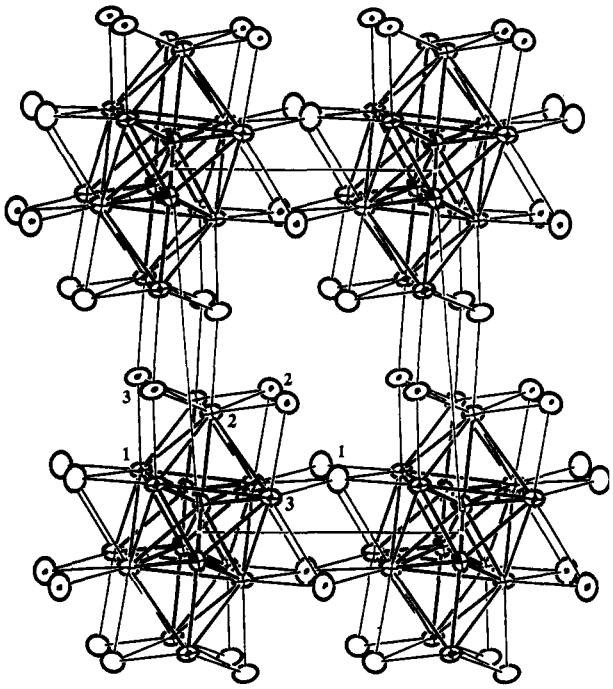

Figure 1. Slightly-off-[010] projection of one cell of the Gd_3I_3Mn structure ($P2_1/m$, *a*-axis horizontal) along the chains, with Gd–Gd and Gd–Mn interactions highlighted. Gd, Mn, and I atoms are represented with crossed, shaded and open (90%) ellipsoids, respectively. All atoms lie on mirror planes at y = 1/4 or 3/4 (atoms dotted). Inversion centers at 0, 1/2, 0 etc. relate labelled atoms to the others in projection.

Gd_3I_3Mn with a significantly smaller *Z* lies near the distorted extreme, but it also exhibits several noteworthy differences.

Figure 1 is a view of Gd_3I_3Mn along the chains, slightly off [010], that illustrates the atom positions, the connectivities, and something of the chain distortions. A summary of pertinent distances and angles is given in Table 3. All atoms lie on mirror planes at $y = 1/4$ or $3/4$, atoms on the latter being distinguished in Figure 1 by a dot. The horizontal Gd1–Gd3 bonds are recognizable as the shared edges within each imagined chain, but because of distortions the edges nominally shared between the chain pairs, Gd1–Gd1, are now 1.0 Å longer than the average of the other near-neighbor distances. (The atoms in the unlabeled half of the double chain at the lower left in the Figure are related to the rest by inversion centers at 0, 1/2, 0, etc.). The side view of a portion of one chain (without iodine) shown in Figure 2 emphasizes how the metal construction can alternatively, and perhaps better, be viewed as two chains of edge-sharing rectangular

Table 3. Important Distances (Å) and Angles (deg) in Gd_3I_3Mn

		Distances[a]	
Gd1–Gd1	(4.774(2))	Gd1–I1[b]	3.216(2)
Gd1–Gd2 (×2)	3.659(2)	Gd1–I3	3.151(3)
Gd1–Gd3	3.895(3)	Gd2–I2 (×2)	3.126(2)
Gd1–Gd3 (×2)	3.731(2)	Gd2–I3 (×2)	3.206(2)
Gd2–Gd3 (×2)	3.770(2)	Gd2–I3[b]	3.413(3)
		Gd3–I1	3.534(3)
Mn–Gd1	2.940(5)	Gd3–I1[b] (×2)	3.332(2)
Mn–Gd1 (×2)	2.903(4)	Gd3–I2	3.221(3)
Mn–Gd2	3.108(5)		
Mn–Gd3 (×2)	2.948(3)	I1–I1 (×2)	4.017(4)
Mn–Gd3	3.230(5)	I1–I2 (×2)	4.070(3)
		I2–I3 (×3)	4.084(3)
Mn–Mn (×2)	2.665(6)		
		Angles	
Gd1–Mn–Gd1 (×2)	125.7(1)	Gd2–Mn–Gd3 (×2)	77.0(1)
Gd1–Mn–Gd1	90.6(1)	Gd3–Mn–Gd3	88.9(1)
Gd1–Mn–Gd2	145.6(2)		
Gd1–Mn–Gd2 (×2)	74.9(1)	Gd1–I1–Gd3 (×2)	101.56(3)
Gd1–Mn–Gd3 (×2)	78.6(1)	Gd1–I1–Gd3 (×2)	174.36(8)
Gd1–Mn–Gd3	78.1(1)	Gd1–I1–Gd1	79.82(6)
Gd1–Mn–Gd3 (×2)	151.8(2)	Gd3–I1–Gd3	76.54(6)

[a] All atoms also have two like neighbors at ±*b*, 4.127(1) Å. Distance limits are 4.10 Å. [b] Interchain bridging distance.

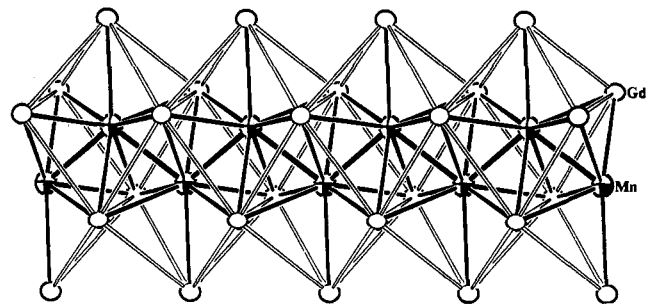

Figure 2. Side view of a portion of one chain in Gd_3I_3Mn (90%). Only metal atoms are shown, with Mn shaded. Note the image of chains of rectangular Gd pyramids held together by a zigzag Mn chain.

pyramids that are displaced from one another by *b*/2 and held base-to-base by the zigzag chain of Mn atoms. The base-to-base superposition is imperfect, reflected by nonequivalent Gd1–Gd1′ and Gd3–Gd3′ cross diagonals in Figure 1, 4.77 vs 5.19 Å, respectively. This example represents the greatest degree of distortion known in the R_3I_3Z family as measured by the smallest difference between these two diagonals or, alternatively, by the decreased R2–Z–R1′ angle from apex to apex of the individual octahedra which is nominally 180° in the ideal case and 145.6° here. The apparent role of the interstitial is more distinctive.

The major changes from known R_3I_3Z structures that appear in this phase when the smaller and electron-poorer Mn is substituted for Ru (or Ir) all appear around the interstitial itself. The heavy interstitials Ru and Ir were found to be displaced toward each other by only about 0.12 Å from the parallel planes defined by the R1–R3 shared edges along each single chain. The resulting Z–Z distances, both close to 3.15 Å, correspond to Pauling metallic bond orders of only 0.08–0.10.[14] With Z = Mn, this displacement from the R1–R3 plane increases greatly to 0.71 Å, so that the Mn–Mn separations within the zigzag chain down the center of the "double chain" (Figure 2), are now only 2.66 Å, equivalent to a Pauling bond order of 0.31 each. It is difficult to understand this marked change as other than a direct result of the encapsulation of atoms that bring one fewer electron each to the bonding scheme.

There are two obvious consequences of the manganese displacement. One is the concomitant increase of about 0.34 Å in the Gd2–Z separation at the cluster apex on the backside. A second is the modest and appropriate increase in the separation between the bases of the square pyramids (Gd1–Gd3′), mainly

Table 4. More Contrasting Distances (Å) in Y_3I_3Ru and Gd_3I_3Mn

	Y_3I_3Ru	Gd_3I_3Mn	Δ
d(R1–R3) (shared edge)	3.500	3.895	0.40
d(R1–R3) (between sq pyr)	3.659	3.731	0.07
$\bar{d}$(R–R)[a] (8 per f.u.)	3.628	3.763	0.135
d_1(R)[b]	3.240	3.243	0.003
d(Z–R1) (×2, along chain)	2.725	2.903	0.18
d(Z–R3) (×2, along chain)	2.776	2.947	0.17
d(Z–R2) (to apex)	2.772	3.107	0.33
$\bar{d}$(Z–R) (CN6[c])	2.774	2.958	0.18
d_1(Z–R)[d]	2.87	2.80	–0.07
d_1(Z)[b]	2.50	2.356	–0.14
d(Z–Z)	3.163	2.664	–0.50
bond order, ea.	0.08	0.31	0.23

[a] The chain repeats at b, 4.18 and 4.13 Å, are omitted. [b] Single bond metallic distances calculated from data in ref 14. [c] Omitting the longer d(Z–R3). [d] Assuming additivity of r_1 values from ref 14.

via Mn–Gd1 contacts between them (Figure 1). A substantial increase in the shared edges R1–R3 (~0.38 Å) also accompanies the closer approach to the interstitials.

These, as well as some other less obvious changes, are unexpected based on comparisons between related structures, as summarized in Table 4 for Y_3I_3Ru vs Gd_3I_3Mn. (We chose the Ru rather than the Ir phase because these interstitials are somewhat closer in size and valence electron count, although the distortion is a little less with the former.) The standard metallic bond distances (based on the elements[14]) describe Gd as only very slightly larger than Y (0.003 Å in diameter), yet the average Gd–Gd distance in this phase (omitting the b repeat) is nearly 0.14 Å greater. Although parallel differences of 0.07 to 0.10 Å in d(R–R) have been noted in the chain structure of the corresponding Gd_2Cl_3 and Y_2Cl_3,[15] these are generally not found in comparable intermetallic compounds like RMn_2 and RCu (CsCl-type).[16] Equally unusual is the 0.18 Å *increase* in $\bar{d}$(Z–R) on going from Y_3I_3Ru to Gd_3I_3Mn even though the d_1(Z) values commonly assigned[17] *decrease* by 0.14 Å between Ru and Mn. It would appear reasonable to conclude that a substantial fraction of the bonding has been transferred from R–R and Z–R to Z–Z or that matrix effects that are not at all obvious maintain larger R–R (and Z–R) interactions in Gd_3I_3Mn. The actual Gd–Mn average distance observed, 2.96 Å (3.00 Å if another Mn–Gd3 is included), is still clearly short when compared with 3.208 Å in $GdMn_2$ ($MgCu_2$-type)[18] and 3.17–3.22 Å in Gd_6Mn_{23}.[19] Comparable differences of 0.1–0.2 Å between R–Z distances in cluster halides and the generally greater separations in analogous intermetallic phases have been noted before in Y_6RuI_{10},[2] $Y_{16}Ru_4I_{20}$,[10] (Sc,Y)$_7$(Fe,Co)I_{12},[1] Zr_6(Fe–Ni)Cl_{15},[20] Th_6(Mn–Ni)Br_{15},[21] and cubic Pr_3PtI_3,[8] but *not*, strangely enough, in monoclinic Pr_3RuI_3,[9] Pr_4RuI_5,[5] and Ca_xPr_{7-x}(Co)I_{12}.[1] A detailed theoretical examination of the bonding characteristics in the R_3I_3Z structure family is probably necessary for a better understanding.

Gd_5I_7Mn. This cubic structure contains only the second example of a centered oligomeric cluster, and with several novel features, but now this is tetrahedrally interbridged by a smaller Gd_4I_8 cluster. The $Gd_{16}Mn_4$ portion of the large cluster is illustrated in Figure 3 in a style that emphasizes its condensed cluster parentage. Important distances and angles in the structure are given in Table 5. The gadolinium polyhedron can be thought of as a truncated tetrahedron $(Gd1)_{12}$ on which the four nominally hexagonal faces have been capped by Gd2 (dotted). The six Gd1–Gd1 separations at the cluster apices that are centered by the $\bar{4}$ axes (one lies vertical in Figure 3) are the longest (3.96 Å). In addition, the average Gd–Gd distances to the six-bonded Gd2 atoms, which have three additional Gd–Mn interactions, are

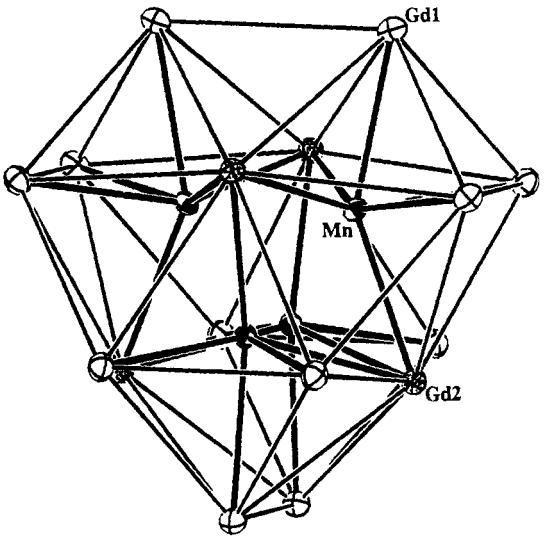

Figure 3. Metal core $Gd_{16}Mn_4$ in the structure of Gd_5I_7Mn with the Gd–Mn interactions highlighted ($4\bar{3}m$ symmetry with $\bar{4}$ vertical). The Mn atoms are shaded, and the Gd2 atoms are dotted. The Gd1 atoms define a truncated tetrahedron (90% probability ellipsoids).

Table 5. Important Distances (Å) and Angles (deg) in Gd_5I_7Mn

		Distances[a]	
Gd1–Gd1 (×2)	3.579(1)	Gd2–Gd1 (×6)	3.843(1)
Gd1–Gd1	3.962(2)	Gd31–Gd1 (×3)	4.770(2)
Gd1–Gd2 (×2)	3.843(1)	Gd31–Gd31 (×3)	3.846(4)
$\bar{d}$(Gd–Gd)	3.761	Gd31–Gd32 (×3)	4.476(8)
		Gd32–Gd1 (×3)	4.115(8)
Gd1–Mn	2.986(3)	Mn–Gd1 (×3)	2.986(3)
Gd2–Mn (×3)	2.923(2)	Mn–Gd2 (×3)	2.923(2)
Mn–Mn (×3)	2.828(8)		
Gd1–I1 (×2)	3.179(1)	I1–Gd1 (×2)	3.179(1)
Gd1–I1[b]	3.361(1)	I1–Gd1[b] (×2)	3.361(1)
Gd1–I21 (×2)	3.167(4)	I1–Gd2	3.169(2)
Gd1–I22 (×2)	3.19(4)	I21–Gd1 (×2)	3.167(4)
Gd2–I1 (×3)	3.169(1)	I21–Gd31	3.199(4)
Gd31–I21 (×3)	3.199(4)	I22–Gd1 (×2)	3.19(1)
Gd31–I3 (×3)	3.016(2)	I22–Gd32	3.02(1)
Gd32–I22 (×3)	3.02(1)	I3–Gd31 (×3)	3.016(2)
Gd32–I3 (×3)	3.441(6)	I3–Gd32 (×3)	3.441(6)
I1–I1 (×2)	4.020(2)		
I1–I2 (×2)	4.003(1)		
I1–I22 (×2)	4.017(1)		
I1–I3	4.036(3)		
I22–I22	4.03(2)		
I1–I22 (×2)	4.017(1)		
		Angles	
Gd1–Gd2–Gd1	55.51(2)	Gd1–Mn–Gd1	73.6(1)
Gd1–Gd2–Gd1	62.07(2)	Gd1–Mn–Gd2	81.11(4)
Gd1–Gd2–Gd1	116.46(1)	Gd1–Mn–Gd2	148.3(2)
Gd1–Gd2–Gd1	157.77(4)		
Gd1–I1–Gd2	74.51(3)	I2–Gd31–I3	88.37(6)
Gd1–I1–Gd2	177.63(5)	I2–Gd31–I3	167.1(1)
Gd1–I2–Gd1	68.81(9)	I2–Gd32–I3	87.94(9)
Gd1–I22–Gd1	68.2(3)	I2–Gd32–I3	169.4(3)
Gd31–I3–Gd31	79.21(9)		
Gd31–I3–Gd32	87.9(1)		

[a] Distance limits are 4.10 Å. [b] Bridging between Gd_{16} clusters.

(14) Pauling, L. *The Nature of the Chemical Bond*; Cornell University Press: Ithaca, NY, **1960**, p 400.
(15) Mattausch, Hj; Hendricks, J. B.; Eger, R.; Corbett, J. D.; Simon, A. *Inorg. Chem.* **1980**, *19*, 2128.
(16) Villars, P.; Calvert, L. D. *Pearson's Handbook of Crystallographic Data for Intermetallic Phases*, 2nd ed.; American Society for Metals: Metals Park, OH, 1991; Vols. 3 and 4.
(17) Pearson, W. B. *The Crystal Chemistry and Physics of Metals and Alloys*; Wiley-Interscience: New York, 1972, p 151.
(18) Slebarski, A. *J. Less-Common Met.* **1980**, *72*, 231.
(19) Wang, F. E.; Gilbrich, J. V.; Ernst, D. W.; Hubbard, W. M. *Acta Crystallogr.* **1964**, *17*, 931.
(20) Zhang, J.; Corbett, J. D. *Inorg. Chem.* **1991**, *30*, 431.
(21) Böttcher, C.; Simon, A.; Kremer, R. K.; Buchkremer-Hermanns, H.; Cockcroft, J. K. *Z. Anorg. Allg. Chem.* **1991**, *589/599*, 25.

characteristically longer than those between the five-bonded Gd1 atoms with only one Gd–Mn bond. The cluster in the tetragonal $Y_{16}I_{20}Ru_4$[10] exhibits just $\bar{4}2m$ (D_{2h}) symmetry, while the present cluster has full $\bar{4}3m$ (T_d) symmetry. (The 3-fold axes pass through Gd2, the farther Mn atom, and the center of the opposed triangular $(Gd1)_3$ face that originated with truncation.) This cluster can also be described as a tetrahedral Mn_4 that is face capped by Gd2 and in turn centered in a larger $(Gd1)_{12}$ cage, or alternatively, it can be imagined to result from the condensation of four $Gd_6(Mn)I_x$ octahedral clusters. Similar descriptions have been used for the cluster in $Y_{16}Ru_4I_{20}$.

The contrasts between these two oligomers may be most evident when these are described as four condensed octahedra. In contrast to Ru in $Y_{16}Ru_4I_{20}$, the Mn interstitials within the Gd cluster are markedly displaced from the former octahedron centers and toward each other to define an inner Mn_4 cluster with edges of 2.828 Å (bond order 0.165). The imagined shared edges between pairs of these nominal octahedra, Gd2–Gd2, are long (4.90 Å) compared with both those around the polyhedral shell (3.58–3.84 Å) and the equivalent separations $Y_{16}I_{20}Ru_4$ (4.3 Å). A more subtle distortion is observed when comparing the skeletal Gd–Gd contacts with the corresponding Y–Y values. While the average of all R–R distances is substantially the same in these two clusters (3.76 Å), the Gd1–Gd1 contacts around the truncated faces [$(R–R)_{trunc}$] decrease by 0.06 Å on going from Y to Gd ($\bar{d}$ = 3.635 Å vs 3.578(2) Å, respectively), but the other Gd1–Gd1 separations and the Gd1–Gd2 distances increase by 0.06 and 0.05 Å, respectively ($\bar{d}$ = 3.903 Å vs 3.963(2) Å and $\bar{d}$ = 3.789 vs 3.843(1) Å, respectively). On the other hand, the average Gd–Gd and Mn–Gd distances here are within 0.003 Å of those in Gd_3I_3Mn above, as unusual as those appeared to be, so that the differences from so-called standard metal radii noted in Table 4 are at least not quite so exceptional. However, the differences in Mn–Mn separations are appreciable (0.16 Å). The parallel relationships between Y_3I_3Ru and $Y_{16}I_{20}Ru_4$ are also similar in all three respects.

The $Gd_{16}Mn_4$ clusters are of course sheathed by iodine. As shown in Figure 4(left), I1 atoms cap the three alternate Gd1–Gd2–Gd1 faces in the hexagonal pyramids that contain the long Gd1–Gd1 distances. These I1 atoms are also bonded exo to pairs of somewhat more distant Gd1 vertices of adjoining $Gd_{16}Mn_4$ clusters, and vice versa, to give intercluster links similar to those that join vertices of cluster chains of Gd_3MnI_3 (compare Figure 1) and elsewhere.[22] The other equally numerous I2 atoms bridge all edges of the $(Gd1)_3$ faces derived by truncation and are also bonded to a new metal cluster fragment.

The presence of an additional small tetrahedral cluster $(Gd3)_4(I3)_4$ in which I3 caps all faces of the metal unit (Figure 4(right)) is a truly novel feature of this structure. This cluster unit lies at the body center of the primitive cubic lattice defined by $Gd_{16}I_{20}Mn_4$ clusters and is bonded to four such clusters in a tetrahedral arrangement via I2 bridges. Only one of these interconnections is shown in Figure 4. The isolated Gd3 atoms, which also lie on the 3-fold axes, thus have quasi-octahedral environments composed of three I3 atoms in the smaller units (larger ellipsoids) and a trio of the I2 atoms that edge-bridge the truncated $(Gd1)_3$ faces of the larger cluster. The I2 atoms are essentially equidistance from Gd1 and Gd3. The local structure and connectivity of the undistorted minicluster is the same as that of the partially characterized Pr_4I_8 ($Mo_4S_4Br_4$ type)[23] in the $F\bar{4}3m$ supergroup. This primitive cubic lattice here allows two different types of clusters. A formal representation of the composition and connectivity of both clusters in this phase is

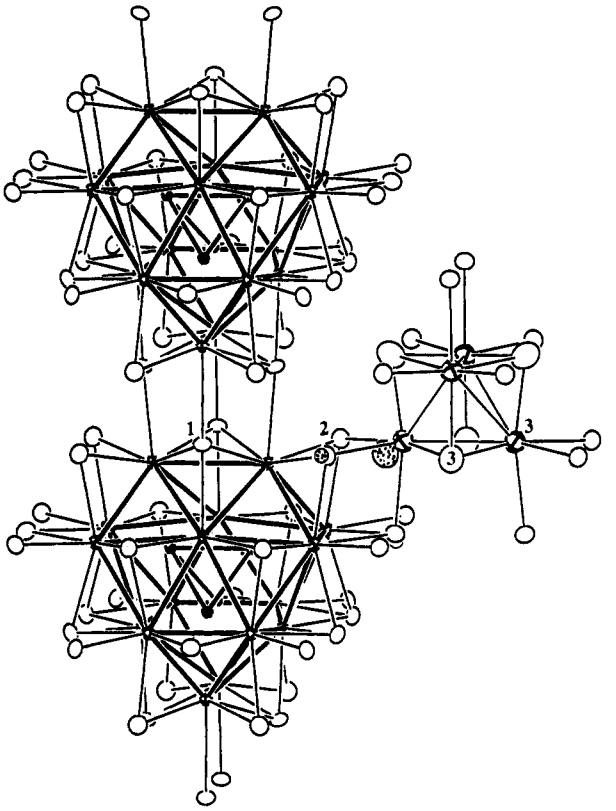

Figure 4. Left: Two $Gd_{16}Mn_4$ clusters centered at 0, 0, 0 and 0, 0, 1 with their iodine sheathing (open ellipsoids) and the $Gd1–I1^{a-i}$ intercluster bridging along the cubic cell axes (vertical). (The second cubic axis is tilted to the right by *ca* 40°.) Right: The $(Gd3)_4(I3)_4$ cluster unit centered at $^1/_2$, $^1/_2$, $^1/_2$ and one of its four bridges to the large clusters via shared $(I2)_3$ atoms. One example of the 25% disorderd Gd23 and the corresponding displaced I22 are shown dotted (see text).

$$[Gd_4(I3)_4(I2)_{12/3}][Gd_{16}Mn_4(I1)_{12}(I2)_{(12\cdot2/3)}] \equiv [Gd_4I_8][Gd_{16}Mn_4I_{20}] \equiv Gd_{20}I_{28}Mn_4$$

if the pairs of somewhat longer I1–Gd1 connections between large clusters are neglected in partitioning the iodine atoms. Finally, it is interesting to note that the complete $(Gd3)_4(I3)_4(I2)_{12}$ diposition is, atom type by atom type, the exact counterpart of the $Mn_4(Gd2)_4(Gd1)_{12}$ core of the large cluster.

However, the small capped tetrahedral cluster $(Gd3)_4(I3)_4(I2)_{12}$ considered up to this point really represents only 75% of the Gd3 refinement result. A second position (Gd32), displaced 0.77 Å along the 3-fold axis away from the small and toward the larger cluster, is occupied the other 25% of the time, randomly in the imposed cubic space group. This displaced Gd32 feature also leads to a comparable minor (I22) component of the I21 atoms that bridge Gd3 to $(Gd1)_3$ and at effectively the same distance therefrom (3.167(4) and 3.19(4) Å for the Gd1–I21 and Gd1–I22 distances, respectively). One example of each is shown dotted in Figure 4. Resolution of any components of I3 that appear to be reflected by a relatively large B_{iso} = 2.43 Å^2 was not possible. In fact, a single solution would not be expected for a superposition of the results of displacement of any one of three neighboring Gd3 atoms, a change which must also to some degree be accompanied by a response of all the I3 and other Gd3 atoms.

We believe that most plausible interpretation of the fractional displacement of Gd32 as refined in the $P\bar{4}3m$ space group is that the crystal actually is a twinned (quadrilled) composite of four possible orientations of the real trigonal structure in the probable space group $R3m$. The displacement of a unique Gd32 atom in the latter would occur along the unique 3-fold axis, the four domains of the rhombohedral structure lying along the cube diagonals in the refined cubic structure. Suitably transformed

(22) Corbett, J. D. in *Modern Perspectives in Inorganic Crystal Chemistry*, Parthé, E. Ed.; NATO ASI Series C; Kluwer Academic Publishers: Dordrecht, The Netherlands, 1992; pp 27–56.
(23) Warkentin, E.; Bärnighausen, H. *Z. Anorg. Allg. Chem.* **1979**, *459*, 187.
(24) Meyer, G.; Meyer, H.-J. *Chem. Mater.* **1992**, *4*, 1164.

diffraction data could not be refined in any one of the possible rhombohedral orientations without evidence of the present disordered Gd32 and I22. However, the quadrilled model seemed clearly indicated by the fact that the disordering, and thence the domain size, was not equal among all four possible rhombohedral orientations (see Experimental Section). Other compounds closely related to Gd_5I_7Mn also exhibit different features of this unusual structure. In addition to the isostructural La_5I_7Mn (as judged by its powder pattern), three scandium analogous have been refined in $P\bar{4}3m$ with essentially the same structure, $Sc_{5-x}Br_7Z$ for x = 0.1–0.2 and Z = Mn, Os, or Ru. But in these cases no *R3* displacement is evident; instead, the position appears to be fractionally occupied, namely by $1 - x$.[25]

The modest distortion of the Gd_4I_8 unit deduced here may be the consequence of a repulsion between the apparently nonbonded Gd(III) atoms (below) in a regular tetrahedron since these would be in close proximity, 3.84 Å, relative to an average distance of only 3.76 Å in the more reduced Gd_{16} cluster with definite metal-metal bonding. Displacement of one vertex in the tetrahedron would remove half of the Gd···Gd interactions therein. The Gd1–Gd32 separations, 4.11 Å, remain relatively long.

Electronic interpretation of the structure of Gd_5I_7Mn requires particular attention to the Mn–Mn interactions. These are 0.16 Å longer than in Gd_3I_3Mn, but each interstitial now has three like neighbors (2.825 Å, total Pauling bond order = 0.50) rather than two (2.665 Å, total bond order = 0.62) in the chain structure. The average Mn–Gd distance is still effectively the same as in Gd_3I_3Mn. A notable contrast occurs relative to $Y_{16}I_{20}Ru_4$. The smaller Mn with one fewer electron appears to develop significant interactions with three like neighbors, as opposed to substantially no Ru–Ru bonding (d = 3.57 Å; bond order ~0.02) in $Y_{16}I_{20}Ru_4$. However, this circumstance is not too distinctive on consideration of the electronic structure of the minicluster.

There are serious problems with an assumption that the smaller Gd_4I_8 unit is neutral and therefore contains Gd(II), whereas its incorporation into this phase has a special significance if we consider it to contain gadolinium(III) and therefore formally to be $Gd_4I_8^{4+}$. A neutral cluster of tetrahedral Gd_4 units is not reasonably bound with only four electrons; instead, upward of 12 (a_1^2,e^4,t_2^6) would be expected.[24] Furthermore, the observed distortion/disorder of Gd3 would serve to destabilize (and split) the would-be bonding orbitals. Thus, the most reasonable assignment of the Gd3 atoms is as normal-valent metals, affording a $(Gd_4I_8)^{4+}(Gd_{16}I_{20}Mn_4)^{4-}$ representation in which the large cluster is now isoelectronic with that in $Y_{16}I_{20}Ru_4$. An extended Hückel band calculation on the structure supports the idea that the $(Gd3)_4$ bonding states are high lying and empty with or without distortion.

Calculations were also performed on both the isolated Gd_{16} cluster as observed and a hypothetical one in which the Mn atoms were moved to positions more closely resembling those in the $Y_{16}I_{20}Ru_4$ cluster in an attempt to understand why the apparently isoelectronic clusters exhibit such structural variations. In contrast to the calculations previously reported for the isolated $Y_{16}(Ru_4)I_{20}I_{12}^{12-}$,[10] ours for $Gd_{16}I_{20}Mn_4^{4-}$ do not indicate a clear separation between R–R; R–Z; and Z–Z-based orbitals. This is in part consistent with the smaller separation between the energies of the Gd and Mn atomic orbitals. Strong Mn–Mn bonding is indicated, with corresponding bond populations of 0.233 (per tetrahedron edge), but these states are not isolated; rather, the a_1, e, and t_2 bonding states show considerable mixing with all of the Gd–Gd cage bonding orbitals with the respective symmetries.

Both the contraction of the Z–Z contracts and the variation within the skeletal R–R distances in $Gd_{16}I_{20}Mn_4^{4-}$ relative to those in $Y_{16}I_{20}Ru_4$ noted above most strongly influence one orbital of a_1 symmetry located near the HOMO–LUMO gap. This orbital exhibits bonding character between Gd1 atoms in the truncated faces [$(R - R)_{trunc}$] and between the interstitial atoms (Z), but it is R–Z antibonding. As the interstitial atoms are moved away from the center of the octahedral cluster fragments and toward each other, this orbital loses R–Z antibonding character while gaining $(R–R)_{trunc}$ and Z–Z bonding, thus stabilizing the a_1 just below the e HOMO and giving a ~0.4-eV gap. However, given that both the Y/Ru and Gd/Mn clusters appear to be isoelectronic, this result implies that $(Gd_5I_7Mn)_4$ should exhibit a degenerate e^2 HOMO. Unfortunately, this can not be readily confirmed owing to gadolinium's paramagnetic core. On the basis of the above orbital arguments, either a larger interstitial or a more condensed rare-earth-metal skeleton would be necessary to destabilize this a_1 orbital and achieve a closed-shell e^4 electronic configuration. The isostructural $(La_5I_7Mn)_4$ and two closely related scandium phases exist,[25] and we are attempting to synthesize these in high yields and purity so that magnetic studies can be performed. Although our calculations resonably describe the observed structural variations, it is unclear as to why a structure with a closed shell electronic structure is evidently not attained. However, this may not be possible in this structure with variations of only a single interstitial type and in the local R_4I_4 cluster structure, each changing the electron count per cluster in multiples of four.

Acknowledgment. The authors are indebted to H. F. Franzen and G. J. Miller for helpful advice. This research was supported by the National Science Foundation, Solid State Chemistry, via Grants DMR-8902954 and -9207361 and was carried out in facilities of the Ames Laboratory, DOE.

Supplementary Material Available: Tables of data collection and refinement details and of anisotropic displacement parameters for Gd_3I_3Mn and Gd_5I_7Mn (2 pages). Ordering information is given on any current masthead page.

(25) Steinwand, S. J.; Martin, J. D.; Corbett, J. D. Unpublished research.